Bare-tether cathodic contact through thermionic emission by low-work-function materials

Xin Chen[a] and J. R. Sanmartín[b]
Departamento de Física Aplicada, Escuela Técnica Superior de Ingenieros Aeronáuticos, Universidad Politécnica de Madrid, Plaza Cardenal Cisneros 3, 28040 Madrid, Spain

(Received 24 April 2012; accepted 9 June 2012; published online 12 July 2012)

A new material, C12A7 : e^- electride, which might present a work function as low as 0.6 eV and moderately high temperature stability, was recently proposed as coating for floating bare tethers. Arising from heating under space operation, current is emitted by thermionic emission along a thus coated cathodic segment. A preliminary study on the space-charge-limited (SCL) double layer in front of the cathodic segment is presented using Langmuir's SCL electron current between cylindrical electrodes and orbital-motion-limited ion-collection sheath. A detailed calculation of current and bias profiles along the entire tether length is carried out with ohmic effects and the transition from SCL to full Richardson-Dushman emission included. Analysis shows that in the simplest drag mode, under typical orbital and tether conditions, thermionic emission leads to a short cathodic section and may eliminate the need for an active cathodic device and its corresponding gas feed requirements and power subsystem, which results in a truly "propellant-less" tether system for such basic applications as de-orbiting low earth orbit satellites. © *2012 American Institute of Physics*. [http://dx.doi.org/10.1063/1.4736987]

I. INTRODUCTION

Electrodynamic tethers are made of conductive wires, which carry currents between the ends. Taking advantage of basic principles of electromagnetism, the tether system exchanges momentum with a planetary magnetosphere and offers the opportunity for in-orbit "propellantless" propulsion around planets with a magnetic field and an ionosphere.

A non-relativistic transformation relates the electric fields, in the frames moving with tether and local ambient plasma[1]:

$$\vec{E}_{TetherFrame} - \vec{E}_{PlasmaFrame} = (\overrightarrow{v_t} - \overrightarrow{v_{pl}}) \times \vec{B}, \qquad (1)$$

where the planetary magnetic field $\vec{B}$ is common in both frames, and $\overrightarrow{v_t}$ and $\overrightarrow{v_{pl}}$ are the velocities of tether and plasma, respectively. In the highly conductive plasma away from the tether, the electric field is negligible in the frame moving with the plasma. Then, the electric field outside the tether yet in the frame of the tether, which is a motional electric field, can be written as

$$\vec{E}_{outside} = \vec{E}_{TetherFrame} = \overrightarrow{E_m} = (\overrightarrow{v_t} - \overrightarrow{v_{pl}}) \times \vec{B}. \qquad (2)$$

The field inside the tether is determined by Ohm's law.

For non-zero orbital inclination or a realistic magnetic model, the projection of $\overrightarrow{E_m}$ along the tether, E_m, drives a current $\vec{I}$, while other components of $\overrightarrow{E_m}$ produce negligible potential difference across the thin tether. An insulated tether with length L, carrying a uniform current, would in turn experience a Lorentz force

$$\vec{F} = L\vec{I} \times \vec{B}. \qquad (3)$$

The power transferred to the tether is thus

$$W_t = L\vec{I} \times \vec{B} \cdot \overrightarrow{v_t}. \qquad (4)$$

In the case of a passive tether system, the net mechanical power extracted from the orbital motion, $W_m = L\vec{I} \cdot \overrightarrow{E_m} = -L\vec{I} \times \vec{B} \cdot (\overrightarrow{v_t} - \overrightarrow{v_{pl}}) > 0$, appears as the current in the tether electric circuit. And the Lorentz force acts as a drag ($W_t < 0$) if $\overrightarrow{v_t}$ is in the same direction as $\overrightarrow{v_t} - \overrightarrow{v_{pl}}$, otherwise a thrust ($W_t > 0$). The component of Lorentz force that is perpendicular to the tether orbital plane, however, may lead a coupled in-plane/off-plane unstable periodic motion.

A standard electrodynamic tether, which carries insulation, collects or rejects electrons through a positively biased anodic end device or a negatively biased cathodic end device, respectively. In the early 1990s, the bare-tether concept was proposed as providing an electron-collecting anode limited by neither space charge nor magnetic guiding effects, to be more effective than large conductive spheres at the tether ends.[2] The small cross-sectional dimension of the tether allows it to collect electrons over the resulting positively biased (anodic) segment as a giant cylindrical Langmuir probe in the orbital-motion-limited (OML) regime. In addition, the collecting area is large because the anodic segment may be many kilometers long.[3]

A standard bare tether emits the full electron current through a low-impedance cathodic device, such as a hollow cathode, located at the cathodic end of the tether. Since the hollow cathode requires a low bias to eject the collected current, the tether bias in the simplest drag mode is positive over most of the tether length, which allows high current and drag.[4]

In the absence of a low-impedance device, current is emitted through ion collection along the negatively biased (cathodic) segment. Ions arrive at the tether following the

[a]Electronic mail: xin.chen@upm.es.
[b]Electronic mail: juanr.sanmartin@upm.es.

OML law, each ion picking up an electron and leaving as a neutral, electrons thus leaking out at the ion impact rate. The current flowing along the tether vanishes at both ends and the tether is said to be completely passive and electrically floating. In this case, under OML electron/ion collection, the anodic-to-cathodic length ratio is low because the ions are much heavier than the electrons, about $\sqrt[3]{m_e/m_i} = 0.03$ for oxygen ions. Therefore, less current is collected compared to a standard bare tether with the same length, and the length-averaged current is reduced. However, if coating with low enough work function is available and the cathodic segment is heated to high-enough temperature, thermionic emission, instead of ion collection, improves efficiency.

A low-work-function electron-emitting material C12A7 : e^- was developed by Hosono's group at the University of Tokyo.[5] Since this material has a work function potentially as low as 0.6 eV, it can emit intense current at temperature about 300 K, well below values (1300–1400 K) required by, say, LaB_6 and CeB_6 (2.7 eV). Williams brought such advances in materials science to the tether community. In work together with Sanmartin and Rand, C12A7:e^- was proposed as coating for floating bare tethers.[6] Thermionic emission along the coated cathodic segment, arising from heating under space operation, might be well more efficient than ion collection.

The C12A7 : e^- electride is derived from the compound $12CaO \cdot 7Al_2O_3$ (C12A7). The crystalline ceramic C12A7 has a naturally formed nanostructure, in which subnanometer-sized cages form a three-dimensional crystal lattice. The unit cell is $[Ca_{24}Al_{28}O_{64}]^{4+}(O^{2-})_2$, composed of two C12A7 molecules. A positively charged lattice framework, as the first term of the chemical formula, contains twelve crystallographic cages, each with a radius of 0.2 nm The extra-framework free oxygen ions $(O^{2-})_2$, clathrated (floating) within two of the twelve cages, can be replaced exclusively by electrons, which results in the formation of the electride $[Ca_{24}Al_{28}O_{64}]^{4+}(e^-)_4$, or C12A7 : e^-. Due to the large lattice spacing, electrons are loosely bound to the crystal lattice, and this inorganic conducting ceramic may have a low work function. An extremely low work function of 0.6 eV was predicted from the field-emission characteristics by Hosono's group at the Tokyo Institute of Technology.[5] Subsequent studies at higher operation temperatures gave a higher value of 2.1 eV,[7] which is still low compared to the state-of-art electron emitting materials, e.g., LaB_6 and CeB_6 with 2.7 eV. The same group evaluated the work function as 2.4 eV by photoelectron yield spectroscopy (PYS) and UV photoelectron spectroscopy (UPS) techniques.[8] Recently, a work function of 0.82 ± 0.1eV has been measured by Williams' group at Colorado State University.[9] Although this work function increased over time, it is thought that this is due to the formation of a contamination layer on the sample surface and removal of the contamination layer would help the material return to the low work function.

Another feature of interest of C12A7 : e^- electride is its high stability compared to the state-of-art electron emitting materials. Finding a material with a sufficiently low work function often results in the compromise of other properties that has led to materials that are consumable, easily poisoned, and susceptible to being sputtered away. For instance, the barium-calcium aluminate impregnated porous tungsten (Ba–W), with a work function of 2.1 eV, is susceptible to both poisoning and high rates of evaporation if operated at high current. For C12A7 : e^- electride, when it is exposed to an ambient atmosphere, the rigid structure of the lattice framework made of Ca–O and Al–O bonds prohibits the diffusion of H_2O and O_2 molecules into a cage to react with the low work-function electrons.[8] As a result, this electron-emitting material is stable up to several hundred degrees Celsius in an ambient environment.[9]

With this low-W coating, each point on the cathodic segment of a kilometers-long floating bare-tether would emit current as if it were part of a hot cylindrical probe uniformly polarized at the local tether bias, under 2D probe conditions that are also applied to the anodic-segment analysis. Around a negatively biased probe with intense thermionic emission, immersed in plasma, a double layer (DL) would be established with electrons being emitted from the tether and ions coming from the ambient plasma. The thermionic current density, varying along the cathodic segment, might follow two distinct laws under different conditions, space-charge-limited (SCL) or full Richardson-Dushman.

The first analysis of DL was conducted by Langmuir[10] for an one-dimensional, planar DL, giving the ratio of ion to electron SCL current density. Although the result is not self-consistent, it is a good approximate for a strong DL. The computations of space charge, electric field, or potential inside the planar DL in front of a hot cathode were later carried out using a fluid model.[11–13] The SCL, counter-flowing monoenergetic ion and electron currents between two spherical surfaces, which also forms a DL, was studied by Wei and Wilbur.[14] For cylindrical DL, not many studies have been found. Chang and Bienkowski[15] developed a method for the SCL DL in front of spherical and cylindrical probes (positively or negatively biased), using orbital motion theory, but under the assumption of Debye length being much smaller than probe radius. Although the attracted particles were considered monoenergetic, this paper casts light on the problem to find a self-consistent DL solution. Recently, Fruchtman *et al.*[16] presented a two-scale analysis for a DL in front of a negatively biased emissive cylindrical probe, but, with vanishing net current.

In the case of the cathodic emission around the floating bare tether, of which each point is considered as a uniformly polarized probe, high plasma-to-tether potential results in a thick 2D cylindrical DL carrying currents, which has not been resolved in previous works. Also, the transition between SCL and non-SCL emission has not been analysed, which is important for floating bare-tether analysis. In this work, as a preliminary study on the two dimensional SCL DL, using the rough model in the work of Williams *et al.*,[6] we calculate the emission current inside the DL by patching Langmuir's SCL electron current between cylindrical electrodes[17] and OML ion-collection sheath.[3] The Richardson-Dushman emission law is then used beyond the SCL regime. Self-consistent current collection and emission along the entire bare tether, taking into account ohmic effects, are studied. The transition between different cathodic emission regimes is identified by a transition in tether length. Basic

features in the balance of currents are presented and discussed considering typical space parameters.

II. THERMIONIC EMISSION AROUND A NEGATIVELY BIASED CYLINDRICAL PROBE

When the plasma-to-probe bias reaches some high enough value, the thermionic-emission current density—limited by the emitter temperature T—follows the Richardson-Dushman's law with Schottky effect (RDS current density):

$$j_{RDS}(T,W,E_s) = j_0(T,W) \times S(T,E_s), \tag{5}$$

where W is the work function of the material. The Richardson-Dushman current density is

$$j_0(T,W) = \frac{4\pi m_e e k^2}{h^3} T^2 \exp\left(-\frac{W}{kT}\right), \tag{6}$$

where k is the Boltzmann constant and h is the Plank constant. The Schottky enhancement factor S is given by

$$S(T,E_s) = \exp\left(\frac{e}{kT}\sqrt{\frac{eE_s}{4\pi\varepsilon_0}}\right), \tag{7}$$

where ε_0 is the vacuum permittivity and E_s is a (moderate) electric field established at the emitter surface.

However, at a lower plasma-to-probe bias, the electron emission at the emitter surface is limited by the electric field at the emitting surface which arises from the space charge of the emitted electrons. This current is referred to as SCL current, being lower than RDS current. In this preliminary study on the SCL double layer, we shall make use of work by Langmuir and Blodgett on SCL current emitted by a hot inner cylinder to a cold positively biased cylinder.[17]

For a negatively biased cylindrical hot cathode which has a radius r_0 and emits electrons outwards with negligible initial velocity, Langmuir described the SCL electron current density per unit length as

$$i_l = 4\pi\varepsilon_0 \times \frac{2\phi(r)}{9r[\beta(r/r_0)]^2} \times \sqrt{\frac{2e\phi(r)}{m_e}} \; constant\ along\ the\ path, \tag{8}$$

where $\phi(r) > 0$ is the potential relative to the cathode at a distance r to the cylindrical axis. The value of β is zero for $r/r_0 = 1$ and increases until it approximates unity for $r/r_0 > 10$. Evaluating the current at the outer anodic cylinder with radius $r_{an} > 10r_0$, one sets $\beta \approx 1$ and the current per unit length becomes

$$i_l = 4\pi\varepsilon_0 \times \frac{2\phi(r_{an})}{9r_{an}} \times \sqrt{\frac{2e\phi(r_{an})}{m_e}}. \tag{9}$$

In the case of the DL around a hot cylindrical probe negatively biased with respect to ambient plasma, the coaxial cylindrical sheath will represent an anode collecting the electron current as described in Eq. (9) and emitting ions inwards, with most of the potential drop, at the high bias of interest, taking place inside the sheath,

$$r_{an} \approx r_{sh}, \quad \phi(r_{sh}) \approx -\Delta V, \tag{10}$$

where $\Delta V < 0$ is the probe-to-plasma bias. If one neglects the ion space charge, Eq. (9) can be used to evaluate the total SCL current inside the sheath, as the ion current is supposed to be negligible. We still assume that the sheath radius is indeed much larger than the probe radius ($r_{sh} \gg R \equiv r_0$). While the ion space charge is neglected, we go further in simplifying this preliminary analysis by using the model for r_{sh} arising from ion OML collection. The maximum radius R_{max} for the OML regime to be hold depends on λ_{Di}, $e\Delta V/kT_i$, and T_i/T_e. For a typical ion-to-electron temperature ratio $T_i/T_e \approx 1$, the maximum radius is close to the Debye length ($R_{max} \approx \lambda_{Di}$), being weakly dependent on $e\Delta V/kT_i$.[3] Considering $T_i/T_e \approx 1$ and $R = \lambda_{Di} \approx R_{max}$, the sheath radius r_{sh} reads

$$r_{sh} = \frac{R}{\sqrt{\sigma_1}}\sqrt{\frac{-e\Delta V}{kT_i}}, \tag{11}$$

where σ_1 is a constant with a value 0.24.[18] Then, the SCL current per unit length becomes

$$i_{SCL} = \frac{8\pi\varepsilon_0}{9}\sqrt{\sigma_1}\left(\frac{-\Delta V}{R}\right)\sqrt{\frac{2kT_e}{m_e}}. \tag{12}$$

Although the Langmuir theory describes the emitted electrons and the OML theory describes independently the incoming ions, this preliminary analysis may give correct magnitude for the DL considering both species.

III. FLOATING BARE TETHERS WITH THERMIONIC EMISSION

As shown in Fig. 1, the anodic segment AB collects electrons from the ambient plasma until the zero-bias point B. For a round tether with a radius R less than or equal to R_{max}, it can be assumed that the current collection follows the high-bias OML theory ($\Delta V = V_t - V_p \gg kT_e \approx 0.1$eV) except in regions very close to B. Again, for $T_i/T_e \approx 1$ and $R = R_{max}$, the OML current density at distance y from A then reads

$$j_{OML}(y) = \frac{en_\infty}{\pi}\sqrt{\frac{2e\Delta V(y)}{m_e}}, \tag{13}$$

where n_∞ is the unperturbed plasma density.

At the cathodic segment immediately after B, with a low plasma-to-tether bias, the current is emitted at the rate of SCL current i_{SCL} in Eq. (12). In regions very close to B, although this high-bias approximation may not be correct, the current emission in these regions is negligible. If the plasma-to-tether bias reaches a certain value while increasing along the tether, current is emitted at the rate of RDS current density j_{RDS} in Eq. (5).

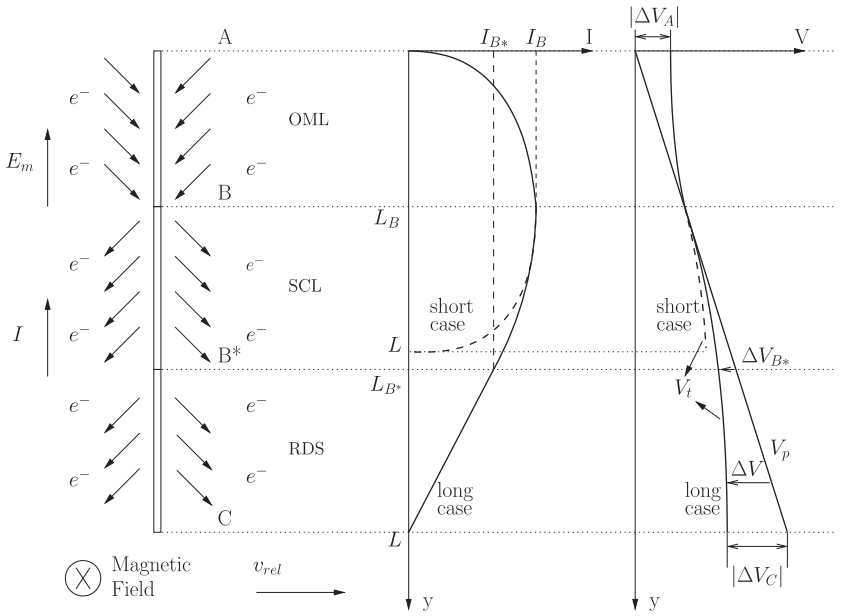

FIG. 1. Scheme of plasma potential V_p, tether potential V_t, and current I along a floating bare tether with thermionic emission, operating in drag mode. To show each segment clearly, this figure is not drawn in scale.

In some circumstances, tethers operate in highly inclined orbits or at high altitude will not be able to collect a very significant electron current by the anodic segment, as if the tether were *short*. In this *short* case, the current can be emitted fully just by a SCL segment, as the dashed line in Figure 1. If more current is collected by the anodic segment, the cathodic segment might first emit current by a SCL segment up to the transition point B*, beyond which current is emitted by a RDS segment, as the full line in Fig. 1. In this *long* case, j_{RDS} and $i_{SCL}/2\pi R$ are identical at point B*.

Besides the anodic collection, the transition between two cases is also determined by the cathodic emission which is critically related to the work function and the temperature of the emitting surface. The RDS current density, if being low due to high work function or low temperature [Eq. (5)], would move upward the transition point B* and prevent the emission from further increment, which thus reduces the emission efficiency and drag production. Thus, the new low-W material is important because it allows reaching desired emissions at lower temperatures. Tether temperature is determined from a thermal balance, where the heating mainly arises from ohmic dissipation and solar irradiation. Note that in going from the eclipse to the non-eclipse phase in orbit, cathodic electron emission will increase because solar heating dominates ohmic heating,[1] while anodic electron collection will also increase along with ambient plasma density n_∞. In this work, the temperature is considered as constant along the tether and thermal balance is left to future analysis.

The floating bare tether system with thermionic emission can self-consistently adjust the position of B, and of B* if present, to establish a current that vanishes at both ends. Detailed calculations for each segment and each case are carried out in Secs. IV and V. For simplicity, the Schottky effect is assumed negligible.

IV. THE ANODIC-SEGMENT COLLECTION A-B

Under OML collection, Eq. (13), the current variation along the AB segment follows

$$\frac{\mathrm{d}I}{\mathrm{d}y} = 2eRn_\infty\sqrt{\frac{2e\Delta V}{m_e}}. \tag{14}$$

Accounting for ohmic effects, the local bias varies throughout the length of the tether following the equation:

$$\frac{\mathrm{d}\Delta V}{\mathrm{d}y} = \frac{I}{\sigma_c A_t} - E_m, \tag{15}$$

where A_t is the tether cross-sectional area and σ_c is the tether conductivity. Three dimensionless variables are defined:

$$\xi = \frac{y}{L^*}, \quad i = \frac{I}{I^*}, \quad \phi = \frac{\Delta V}{E_m L^*}, \tag{16}$$

where we introduce the short-circuit current $I^* = \sigma_c A_t E_m$ and a characteristic length L^* defined as

$$L^* \equiv l^{1/3} \times R^{2/3}, \tag{17}$$

with l given by

$$l = \frac{9\pi^2 m_e \sigma_c^2 E_m}{128 e^3 n_\infty^2}. \tag{18}$$

At particular values, typical of tether applications ($n_\infty \approx 3\times 10^{11}/m^3$ and $E_m \approx 150\mathrm{V/km}$) l is about $3.1\times 10^{17}\mathrm{m}$. As a result of ohmic effects, the maximum current that can be collected by the tether is the short-circuit current I^*, which limits i to a range $0 < i < 1$. Thus, Eqs. (14) and (15) become

$$\frac{\mathrm{d}i}{\mathrm{d}\xi} = \frac{3}{4}\phi^{1/2}, \tag{19}$$

$$\frac{\mathrm{d}\phi}{\mathrm{d}\xi} = i - 1, \tag{20}$$

with the latter holding all along the tether. The entire solution can then be given in terms of a single free parameter,

say ϕ_A. An immediate first integral of Eqs. (19) and (20) is $i^2 - 2i - \phi^{3/2} = C$, where C is a constant. After substituting the tip values ($i=0$, $\phi = \phi_A$ at $\xi = 0$; $i = i_B$, $\phi = 0$ at $\xi = \xi_B$), C is evaluated as $C = {i_B}^2 - 2i_B = -{\phi_A}^{3/2}$ with ϕ_A lying in the range $0 < \phi_A < 1$. Then, one has the current profile in the anodic segment:

$$i = 1 - \sqrt{1 - {\phi_A}^{3/2} + \phi^{3/2}}, \tag{21}$$

and the current at B:

$$i_B = 1 - \sqrt{1 - {\phi_A}^{3/2}}. \tag{22}$$

Substituting Eq. (21) into Eq. (20) and integrating with $i=0$ and $\phi = \phi_A$ at $\xi = 0$ yields the potential bias profile at the anodic segment:

$$\xi = \int_{\phi}^{\phi_A} (1 - {\phi_A}^{3/2} + \phi^{3/2})^{-1/2} \mathrm{d}\phi. \tag{23}$$

Then, the anodic-segment length can be written in terms of ϕ_A:

$$\xi_B(\phi_A) = \int_{0}^{\phi_A} (1 - {\phi_A}^{3/2} + \phi^{3/2})^{-1/2} \mathrm{d}\phi. \tag{24}$$

For different values of ϕ_A, the current profile and potential bias profile are shown in Fig. 2. If the tether length is very large, $L \gg L^*$, the total collected current approaches the short-circuit current, $i_B \to 1$, corresponding to dominant ohmic effects. Then, both ϕ_A and ξ_B approach limits

$$\lim_{i_B \to 1} \phi_A = 1, \quad \lim_{i_B \to 1} \xi_B = 4. \tag{25}$$

When i_B is very close to unity, V_t and V_p meet at B being nearly parallel to each other, as in Fig. 2 the ϕ curve meets with the line $\phi = 0$ nearly tangentially. Note that i_B can only approach unity, other than being equal to unity. If $i_B = 1$, the tether is zero-biased at B with the derivative of the bias being zero, which cannot provide the negative bias after B for current emission.

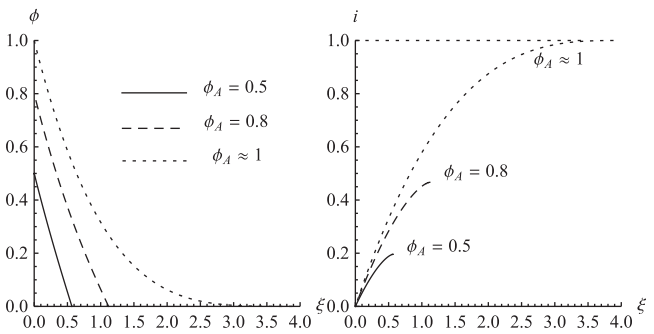

FIG. 2. Tether-to-plasma bias profile and current profile along the anodic segment.

V. THE CATHODIC-SEGMENT EMISSION

Along the SCL segment, Eq. (12) gives the current variation:

$$\frac{\mathrm{d}I}{\mathrm{d}y} = \frac{8\pi\varepsilon_0}{9}\sqrt{\sigma_1}\frac{\Delta V(y)}{R}\sqrt{\frac{2kT_e}{m_e}}. \tag{26}$$

Using the dimensionless variables in Eq. (16) together with a dimensionless parameter to gauge the SCL emission

$$k_s = \frac{2L^*}{3R}\left(\frac{2\varepsilon_0}{R\sigma_c}\right)^{1/2}\left(\frac{2kT_e\sigma_1}{m_e}\right)^{1/4}, \tag{27}$$

the current variation along the SCL segment becomes

$$\frac{\mathrm{d}i}{\mathrm{d}\xi} = {k_s}^2\phi. \tag{28}$$

In the *long* case, when more current is collected, a SCL segment is followed by a RDS segment, along which the current varies as

$$\frac{\mathrm{d}I}{\mathrm{d}y} = -2\pi R j_0, \tag{29}$$

where Schottky effect is assumed negligible ($j_{RDS} = j_0$). Introducing a dimensional parameter to gauge the RDS emission

$$k_t = \frac{2j_0L^*}{\sigma_c R E_m}, \tag{30}$$

the current variation along the RDS segment becomes

$$\frac{\mathrm{d}i}{\mathrm{d}\xi} = -k_t. \tag{31}$$

A. The short case B–C

In the *short* case, Eqs. (20) and (28) hold all the way to the cathodic end C. After an immediate first integral and substituting the tip values at both ends of BC ($i = i_B$, $\phi = 0$ at $\xi = \xi_B$; $i=0$, $\phi = \phi_C$ at $\xi = \xi_C$), it gives ϕ_C and the current profile at the SCL segment:

$$\phi_C = -\frac{{\phi_A}^{3/4}}{k_s}, \tag{32}$$

$$i = 1 - \sqrt{1 - {\phi_A}^{3/2} + {k_s}^2\phi^2}. \tag{33}$$

Substituting Eq. (33) into Eq. (20), and integrating from $i = i_B$, $\phi = 0$ at $\xi = \xi_B$, the bias profile at the SCL segment can be written in a reverse way as

$$\xi = \xi_B + \frac{1}{k_s}\mathrm{arcsinh}\left(\frac{-k_s\phi}{\sqrt{1 - {\phi_A}^{3/2}}}\right). \tag{34}$$

Using Eq. (24), the tether length can be associated to ϕ_A as follows:

$$\frac{L}{L^*} = \xi_C = \xi_B(\phi_A) + \frac{1}{k_s}\operatorname{arcsinh}\left(\frac{{\phi_A}^{3/4}}{\sqrt{1-{\phi_A}^{3/2}}}\right). \tag{35}$$

This relationship shows that, for environmental, geometric and material tether parameters within certain domain, ϕ_A is a function of L, $\phi_A = f(L)$. So, to discuss the dependence of current emission/collection on ϕ_A is equivalent to discuss the dependence on L. Equation (35) also tells that in the case of dominant ohmic effects, since ϕ_A approaches unity, the tether length can be very large as $\xi_C \to \infty$. Using Eq. (20), the average current over the overall tether length can be calculated as

$$i_{av} = \int_0^{\xi_C} i/\xi_C \mathrm{d}\xi = \int_0^{\xi_C} (1 + \mathrm{d}\phi/\mathrm{d}\xi)/\xi_c \mathrm{d}\xi = 1 + \frac{\phi_C - \phi_A}{\xi_C}. \tag{36}$$

Therefore, the average current in the *short* case is

$$i_{av} = 1 - \frac{{\phi_A}^{3/4}/k_s + \phi_A}{\xi_C}. \tag{37}$$

Finally, in the *short* case, if ξ_C is so large that the current collection falls into the case of dominant ohmic effects, the cathodic-segment magnitudes tend to their limits:

$$\lim_{i_B\to 1} \xi_{BC} = \lim_{i_B\to 1}(\xi_C - \xi_B) = \infty,$$
$$\lim_{i_B\to 1} \phi_C = -\frac{1}{k_s}, \quad \lim_{i_B\to 1} i_{av} = 1. \tag{38}$$

B. The long case B–B*–C

In the *long* case, the cathodic-segment emission switches from SCL current to RDS current at B*. Thus, equalizing the RHS of Eqs. (28) and (31), one has the bias at B*,

$$\phi_{B^*} = -\frac{k_t}{{k_s}^2}. \tag{39}$$

The current and bias profiles along this SCL segment BB* are the same as those described by Eqs. (33) and (34). The SCL-segment magnitudes can now be written down in terms of ϕ_A as

$$i_{B^*} = 1 - \sqrt{1 - {\phi_A}^{3/2} + (k_t/k_s)^2}, \tag{40}$$

$$\xi_{B^*} = \xi_B + \frac{1}{k_s}\operatorname{arcsinh}\left(\frac{k_t/k_s}{\sqrt{1-{\phi_A}^{3/2}}}\right). \tag{41}$$

Along the RDS segment B*C, the first integral of Eqs. (20) and (31), together with the tip values ($i = i_{B^*}$, $\phi = \phi_{B^*}$ at $\xi = \xi_{B^*}$; $i = 0$, $\phi = \phi_C$ at $\xi = \xi_C$), gives the current and bias profiles along B*C:

$$i = 1 - \sqrt{1 - {\phi_A}^{3/2} - (k_t/k_s)^2 - 2k_t\phi}, \tag{42}$$

$$\xi = \xi_{B^*} - \frac{1}{k_t}\sqrt{1 - {\phi_A}^{3/2} + (k_t/k_s)^2} + \frac{1}{k_t}\sqrt{1 - {\phi_A}^{3/2} - (k_t/k_s)^2 - 2k_t\phi}. \tag{43}$$

The overall length of the tether ξ_C and the cathodic end bias ϕ_C are found as

$$\xi_C = \xi_{B^*} - \frac{1}{k_t}\sqrt{1 - {\phi_A}^{3/2} + (k_t/k_s)^2} + \frac{1}{k_t}, \tag{44}$$

$$\phi_C = -\frac{{\phi_A}^{3/2}}{2k_t} - \frac{k_t}{2{k_s}^2}. \tag{45}$$

Again, in the dominant ohmic effects limit, $\phi_A \to 1$, the tether length thus being very large, we have $\xi_C \to \infty$ in this *long* case. The average current, using Eq. (36), then becomes

$$i_{av} = 1 - \left(\frac{{\phi_A}^{3/2}}{2k_t} + \frac{k_t}{2{k_s}^2} + \phi_A\right)\Big/\xi_C. \tag{46}$$

Finally, in the *long* case, if ξ_C is so large that current collection falls into the case of dominant ohmic effects, the cathodic-segment magnitudes tend to their limits as

$$\lim_{i_B\to 1} \xi_{BB*} = \infty, \quad \lim_{i_B\to 1} \xi_{B*C} = -\frac{1}{k_s} + \frac{1}{k_t},$$
$$\lim_{i_B\to 1} \phi_C = -\frac{1}{2k_t} - \frac{k_t}{2{k_s}^2}, \quad \lim_{i_B\to 1} i_{av} = 1. \tag{47}$$

C. The short/long cathodic-segment transition

If $k_t > k_s$, the maximum RDS segment length $\lim_{i_B\to 1} \xi_{B*C}$ is negative as shown in Eq. (47), which tells that the tether would always work in the short case, regardless of the tether length. Under the condition $k_t < k_s$, if the tether falls into the *long* case, the value of ϕ_C in Eq. (45) must be less than ϕ_{B^*} in Eq. (39) as the probe-to-plasma bias decreases throughout the tether as in Eq. (20) and Fig. 1. Thus, the condition for a bare tether to work in the *long* case is

$$\phi_A \geq (k_t/k_s)^{4/3}, \tag{48}$$

where the value of k_t/k_s, as found from Eqs. (27) and (30), reads

$$k_t/k_s = \frac{3j_0}{E_m\sigma_c}\left(\frac{R\sigma_c}{2\varepsilon_0}\right)^{1/2}\left(\frac{m_e}{2kT_e\sigma_1}\right)^{1/4}. \tag{49}$$

Substituting $\phi_A = (k_t/k_s)^{4/3}$ into Eq. (35), with $\xi_B(\phi_A)$ given in Eq. (24), yields the shortest length for a tether to work in the *long* case:

$$L_{tr} = L^* \times \int_0^{(k_t/k_s)^{4/3}} [1 - (k_t/k_s)^2 + \phi^{3/2}]^{-1/2}\mathrm{d}\phi + L^* \times \frac{1}{k_s}\operatorname{arcsinh}\left[\frac{k_t/k_s}{\sqrt{1-(k_t/k_s)^2}}\right]. \tag{50}$$

TABLE I. The short/long cathodic-segment transition.

Conditions	Case
$k_t/k_s > 1$, any L	Short
$k_t/k_s < 1, L < L_{tr}$	Short
$k_t/k_s < 1, L > L_{tr}$	Long

As a conclusion, the conditions of the *short*/*long* cathodic-segment transition is shown in Table I.

VI. DISCUSSION

Let us discuss the results with some typical data in space: $\sigma_c \simeq 3 \times 10^7 \mathrm{S/m}$ for aluminium, $kT_e \approx kT_i \approx 0.1\mathrm{eV}$, a low day density $n_\infty \approx 3 \times 10^{11}/\mathrm{m}^3$, $R = \lambda_D \approx 4.29\,\mathrm{mm}$, and $\sigma_1 \approx 0.24$. The conductivity of the aluminium tether would remain unchanged with this thin coating. For a vertical tether in LEO (low earth orbit) equatorial orbit and a nontilted centered magnetic dipole model, a typical motional field lying along the tether reads $E_m = v_t B \approx 7.5\,\mathrm{km/s} \times 2000\mathrm{T} = 150\,V/\mathrm{km}$, with $\vec{B}$ being perpendicular to the tether orbital plane and the resultant current $\vec{I}$. A tentative daytime temperature for the tether $T = 300\,\mathrm{K}$ is used. Different values of work function (0.6 eV, 0.65 eV, and 0.7 eV) are considered for the $\mathrm{C12A7 : e^-}$ coating. We then have $L^* = 17.94\,\mathrm{km}$ and $k_s = 9.18$, both independent of W. The Lorentz force exerted on the tether, calculated as $F = \int \vec{I} \times \vec{B}\mathrm{d}y = \int BI\mathrm{d}y = BLi_{av}I^*$, is shown in Table II for different values of tether length.

For $W = 0.6\,\mathrm{eV}$, one has $k_t = 14.35 > k_s$ and the tether always working in the *short* case regardless of tether length (Fig. 3(a)). A slight increase in the work function, say $W = 0.65\mathrm{eV}$ (Fig. 3(b)) or $W = 0.7\mathrm{eV}$ (Fig. 3(c)), results, however, in $k_t = 2.07 < k_s$ and a transition in tether length beyond which the tether works in the *long* case $L_{tr} = 2.96\mathrm{km}$ ($\xi_{Ctr} = L_{tr}/L^* = 0.16$), or $k_t = 0.52 < k_s$ and $L_{tr} = 0.25\mathrm{km}$ ($\xi_{Ctr} = 0.014$). The short/long cathodic-segment transition is sensitive to the work function. This is because the work function influences the transition conditions in Table I and the transition length in Eq. (50) through the ratio k_t/k_s—the greater the ratio is, the greater the value of L_{tr} is, or even there is not a transition length for long case to be present—and the ratio k_t/k_s [see Eq. (49)] is proportional to j_0 and thus proportional to the exponential term $\exp(-W/kT)$, being sensitive to the work function.

As mentioned at the beginning of this article, a small cathodic-to-total length ratio $(L - L_B)/L$ would correspond to efficient cathodic emission. Shown in Figs. 3(a) and 3(b) for $W = 0.6\mathrm{eV}$ and $W = 0.65\,\mathrm{eV}$, respectively, the ratio first decreases rapidly with the increase of the total tether length down to around 15%, which is indeed small and implies quick current emission from a short segment at the cathodic end of the tether. However, as mentioned, the current emission efficiency is very sensitive to the work function of the material as the work function determines critically the RDS current density. Shown in Fig. 3(c) for $W = 0.7\,\mathrm{eV}$, the cathodic segment is around 50% of total length, and, for a given tether total length, the average current is reduced significantly compared to the results for the other two values of work functions.

TABLE II. Lorentz force.

	1 km	5 km	10 km	20 km
0.6 eV	0.02 N	1.1 N	5.8 N	29.5 N
0.65 eV	0.02 N	1.0 N	5.5 N	26.7 N
0.7 eV	0.01 N	0.6 N	2.6 N	11.8 N

If the tether length is further increased, $L \gg L^*$, the tether falls into the case of dominant ohmic effects, $i_B \approx 1$, and the cathodic-to-total length ratio is increased (Fig. 3) because the SCL segment length keeps increasing while the OML segment length is limited. The cathodic bias $|\phi_C|$ is limited to $1/k_s$ for $W = 0.6\,\mathrm{eV}$ as in the *short* case or limited to $(1/2k_t) + k_t/2k_s{}^2$ for $W = 0.65\,\mathrm{eV}$ as in the *long* case, both being much smaller than ϕ_A as shown in Figs. 3(a) and 3(b). As a result, the plasma and tether potential lines move close to each other, covering most of the cathodic segment, and the current decreases to zero rapidly at the short end of the tether. Thus, a long segment possessing the near short-circuit current tells an efficient current emission in the case of dominant ohmic effects. Again, for $W = 0.7\,\mathrm{eV}$, $|\phi_C|$ increases to a value larger than ϕ_A (Fig. 3(c)), as opposite lower W values, which prevents the cathodic segment from possessing a long section with the short-circuit current and thus the current emission is much less efficient.

We have considered a round-wire radius $R = \lambda_D$ throughout for simplicity; with R_{max} near λ_D independent of bias for $T_i = T_e$, we then have r_{sh} as given by Eq. (11) with $\sigma_1 \approx 0.24$ and $R = \lambda_D$. This results in too heavy tethers, however, for $\mathrm{R} = 4.3\,\mathrm{mm}$, an aluminum wire just 1 km long would be 157 kg heavy. In the case of a sensible radius well below λ_D, one must use a more complex sheath-radius law given in Refs. 18 and 19. Alternatively, one can consider a tether of thin-tape cross section and width w. Round-wire OML results hold for tapes with perimeter $2w$ replacing $2\pi R$ or $w = \pi R$. Further, the maximum width for OML current to hold is $w_{max} = 4R_{max}$.[3] A tape 0.1 mm thick and 15 mm wide say, roughly satisfying the above, would only be around 4 kg heavy for 1 km length. The detailed dependence of SCL current on the electron emitter being cylindrical, through the $\beta(r_{sh}/r_0)$ function, was lost for $r_{sh} > 10r_0$ ($\beta = 1$), as represented by Eq. (9).

As regards geomagnetic-field effects, the Parker-Murphy 2D canonical upper-bound on current lies well above the OML current if the ratio of tether radius to electron thermal gyroradius R/l_e is small. Detailed analysis shows that both $(R/l_e)^2$ and $(R/\lambda_D)^2$ must be small for such effects to be negligible.[3] In turn, effects of the magnetic field generated by the tether current itself prove negligible for thin-tape tethers because ohmic effects then limit the current in the tether.[20,21]

Due to the tether-to-plasma relative flow, there will be the differences in upstream and downstream structures, as there are also differences in sheath structures around round and thin-tape tethers at rest in the plasma.[3] This need not have an effect in collected current, however. In Ref. 22, it

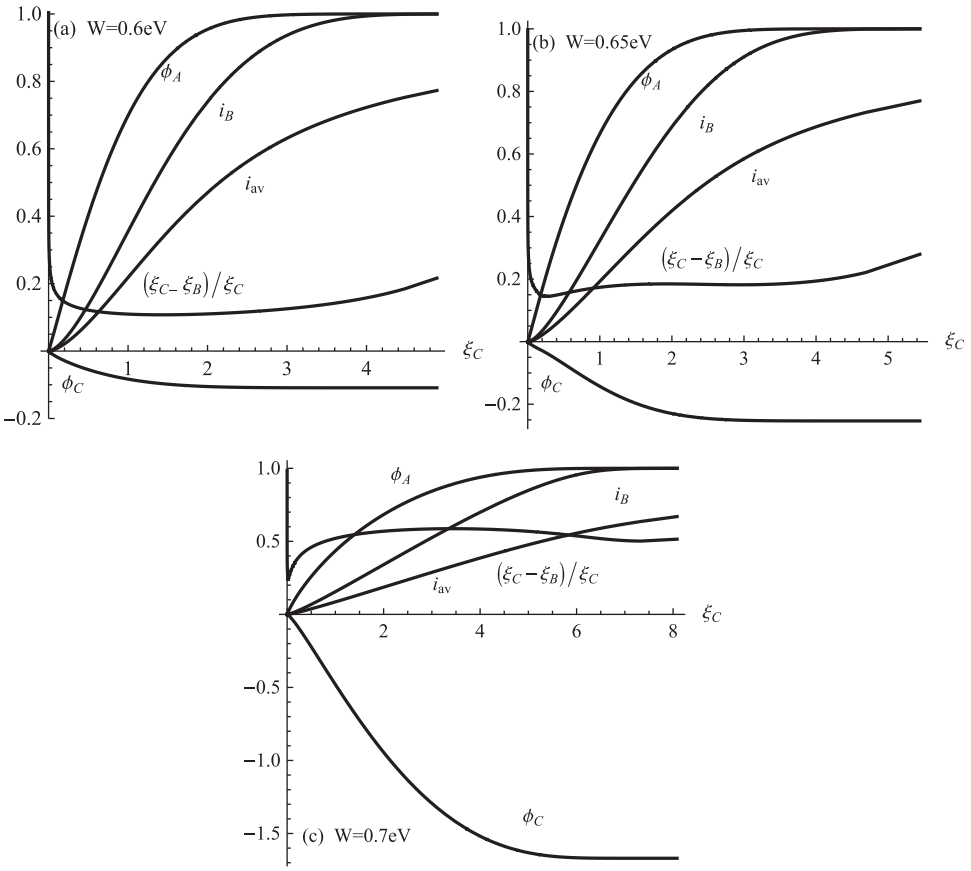

FIG. 3. Anodic bias ϕ_A, collected current i_B, cathodic-to-total length ratio $(\xi_C - \xi_B)/\xi_C$, cathodic bias ϕ_C, and length-averaged current i_{av} are plotted against tether length ξ_C, at the value $k_s = 9.18$, with different work functions: (a) $W = 0.6\,\text{eV}$, $k_t = 14.35$, no ξ_{Ctr}; (b) $W = 0.65\,\text{eV}$, $k_t = 2.07$, $\xi_{Ctr} = 0.35$; (c) $W = 0.7\,\text{eV}$, $k_t = 0.52$, $\xi_{Ctr} = 0.08$.

was shown that the 2D OML current law does not depend on azimuthal symmetry; it just requires that (1) the undisturbed velocity distribution of the attracted species is isotropic, and (2) all orbits traced back in time from the probe reach infinity (there may be no potential barrier for the probe surface). For the no-flow case, condition (2) holds for a round tether with radius below R_{max}. Condition (1) is clearly satisfied for the anodic segment, where electrons are the attracted particles. As regards the cathodic segment, the collected ion current is negligible against the emitted electron current, and only the simplest description was needed.

A basic issue arises, however, from the mesothermal character of the relative flow, which results in the density of ions exceeding n_∞ where rammed back (upstream), and in electron density lying below n_∞ everywhere,[22] breaking quasineutrality in a large upstream region. It has been suggested[23,24] that a fundamental plasma phenomenon, adiabatic electron trapping,[25] might resolve this paradox.

VII. CONCLUSIONS

A new material, C12A7 : e^- electride, with a possible work function as low as 0.6 eV and high-temperature stability, has the potential to allow an efficient floating bare tether system to be developed. Under typical orbital and tether conditions, in the simplest drag mode, thermionic emission along the cathodic segment (with a thin coating of this ultra low-W material) would result in a short cathodic segment, or the short circuit current covering most of the cathodic segment in the case of dominant ohmic effects. When compared to ion collection, thermionic emission leads to much higher drag values and to eliminating the need for an active cathodic device, corresponding gas feed requirements, and power subsystems, which results in a truly "propellant-less" tether system for such basic applications as de-orbiting LEO satellites.

ACKNOWLEDGMENTS

This work was supported by European Commission FP7 Space Project 262972.

[1]J. R. Sanmartin, E. C. Lorenzini, and M. Martinez-Sanchez, J. Spacecr. Rockets **47**, 442–456 (2010).
[2]J. R. Sanmartin, M. Martinez-Sanchez, and E. Ahedo, J. Propul. Power **9**, 353–360 (1993).
[3]J. R. Sanmartin and R. D. Estes, Phys. Plasmas **6**, 395–405 (1999).
[4]E. Ahedo and J. R. Sanmartin, J. Spacecr. Rockets **39**, 198–205 (2002).
[5]Y. Toda, K. Kobayashi, K. Hayashi, S. Ueda, T. Kamiya, M. Hirano, and H. Hosono, Adv. Mater. **16**, 685–689 (2004).
[6]J. D. Williams, J. R. Sanmartin, and L. P. Rand, "Low Work-Function Coating for an Entirely Propellantless Bare Electrodynamic Tether," IEEE Trans. Plasma Sci. **40**(5), 1441–1445 (2012).
[7]Y. Toda, S. W. Kim, K. Hayashi, M. Hirano, T. Kamiya, H. Hosono, T. Haraguchi, and H. Yasuda, Appl. Phys. Lett. **87**, 254103 (2005).
[8]Y. Toda, H. Yanagi, E. Ikenaga, J. J. Kim, M. Kobata, S. Ueda, T. Kamiya, M. Hirano, K. Kobayashi, and H. Hosono, Adv. Mater. **19**, 3564–3569 (2007).
[9]L. P. Rand, J. D. Williams, and R. Hoyt, "Hollow cathode with electride insert," in AIAA-2011-5992, Joint Propulsion Conference, San Diego, CA, 2011.
[10]I. Langmuir, Phys. Rev. **33**, 954–989 (1929).
[11]F. W. Crawford and A. B. Cannara, J. Appl. Phys **36**, 3135–3141 (1965).
[12]P. D. Prewett and J. E. Allen, Proc. R. Soc. London, Ser. A. **348**, 435–446 (1976).
[13]T. Gyergyek, J. Kovacic, and M. Cercek, Phys. Plasmas **17**, 083504 (2010).

[14]R. Wei and P. J. Wilbur, J. Appl. Phys **60**, 2280–2284 (1986).
[15]K. W. Chang and G. K. Bienkowski, Phys. Fluids **13**, 902 (1970).
[16]A. Fruchtman, D. Zoler, and G. Makrinich, Phys. Rev. E **84**, 025402 (2011).
[17]I. Langmuir and K. B. Blodgett, Phys. Rev. **22**, 347–356 (1923).
[18]J. R. Sanmartin, E. Choiniere, B. E. Gilchrist, J. B. Ferry, and M. Martinez-Sanchez, IEEE Trans. Plasma Sci. **36**, 2851–2858 (2008).
[19]R. D. Estes and J. R. Sanmartin, Phys. Plasmas **7**, 4320–4325 (2000).
[20]G. V. Khazanov, N. H. Stone, E. N. Krivorutsky, K. V. Gamayunov, and M. W. Liemohn, J. Geophys. Res. **106**, 10565–10580, doi:10.1029/2000JA000345 (2001).
[21]J. R. Sanmartin and R. D. Estes, J. Geophys. Res. **107**, 1335, doi:10.1029/2002JA009344 (2002).
[22]J. G. Laframboise and L. W. Parker, Phys. Fluids **16**, 629–636 (1973).
[23]T. Onishi, M. Martinez-Sanchez, D. Cooke, and J. R. Sanmartin, "Pic computation of electron current collection to a moving bare tether in the mesothermal condition," in Paper IEPC-01-245, 27th International Electric Propulsion Conference, Pasadena, CA, 2001.
[24]J. R. Sanmartin, "Active charging control and tethers," in *CNES-Space Technology Course: Prevention of Risks Related to Spacecraft Charging, Toulouse, Francia* (Cépaduès-Éditions, 2002), pp. 515–533.
[25]A. V. Gurevich, Sov. Phys. JETP **26**, 575 (1968).